JOURNAL OF ENGINEERING SCIENCES

Volume 9, Issue 1 (2022)

Mandryka A., Majid A. P., Ratushnyi O., Kulikov O., Sukhostavets D. (2022). Ways for improvement of reverse axial pumps. Journal of Engineering Sciences, Vol. 9(1), pp. D14-D19, doi: 10.21272/jes.2022.9(1).d3

Ways for Improvement of Reverse Axial Pumps

Mandryka A.[1*], Majid A. P.[2], Ratushnyi O.[1[0000-0002-3525-0953]], Kulikov O.[1[0000-0001-7222-8766]], Sukhostavets D.[1]

[1] Department of Applied Hydroaeromechanics, Sumy State University, 2, Rymskogo-Korsakova St., 40007, Sumy, Ukraine;

[2] Katex International Suppliers LLC, 2717, Commercial Center Blvd, Katy, TX 77494, USA

Article info:

Submitted: January 27, 2022

Accepted for publication: June 10, 2021

Available online: June 15, 2022

***Corresponding email:**

a.mandryka@pgm.sumdu.edu.ua

Abstract. The article is devoted to a pilot study of the reverse-bladed pump. The characteristics of the reverse bladed pump are the identical parameters on flow, the head, power, energy efficiency on direct and the return operating modes (at rotation of a rotor of the pump both in one and to the opposite side). The model reversible axial pump with two impeller versions was tested on an experimental bench. The impellers were distinguished by the shape of the profile in the blade sections. The model reversible pump was structurally a reversible axial impeller placed in a cylindrical chamber. Studies were carried out at different angles of rotation of the impeller blades. The power characteristics of tested versions of the pump (impeller) at the design and under loading (unstable operation) modes are given. Low efficiency of the tested versions of the reversible pump compared to the conventional axial pumps is noted, primarily due to the strong influence of the secondary gradients of the pressure factor. The second reason is the profile separation of the flow from the blade surface, to which the tested reverse pump screens are predisposed.

Keywords: reversible pump, fluid flow, pressure head, power, energy efficiency.

1 Introduction

In recent years, the development of some industries has required the creation of a fundamentally new class of the centrifugal (dynamic) pumps, so-called reverse pumps, which have the same parameters in terms of flow, pressure, power, efficiency, cavitation qualities in direct and reverse operation modes of operation, i.e., when the rotor rotates in one or the opposite direction.

The reversible pumps are widely used abroad in the chemical, textile industry, shipbuilding, and hydraulic systems of tidal power plants. In domestic practice, there is no production of such pumps, except for two prototypes, which the Kharkiv Polytechnic Institute developed.

Creating reversible dynamic pumps is a complex technical task (due to a number of their features). At the same time, the domestic practice does not have sufficient information on the calculation and design of such pumps, especially their boost elements.

The issue needs a comprehensive, in-depth examination. All this made this research necessary, its tasks and directions, mainly the creation (development) of boost elements.

For this purpose, two reverse impellers RK-1 and RK-2, with specific speed $n_s = 800$, were designed and tested on an experimental bench.

The task of the tests was to study the working process of the impeller for their improved hydraulic qualities. The working process was analyzed based on the characteristics of the elementary grids located on the cylindrical surfaces of the current and the total (integral) characteristics of the impellers.

The impeller RK-1 is designed by the lifting forces method with the correction for the influence of the grid of infinitely thin plates.

The impeller RK-2 is obtained by design optimization on the computer using the straightforward task of lattice theory [1–4], a radical multi-factor experiment [5], and the calculation of profile losses [6–10].

During the design, both impellers were limited: the outer diameter $D = 0.23$ m, the sleeve is cylindrical, the hub-to-tip ratio of 0.61, the radial component of the input velocity $V_{1u} = 0$, and the constant pressure head H along with radius r.

2 Research Methodology

A particular S-shaped profile symmetrical relative to its geometric center is taken as vane sections for RK-1 [10, 11] (a necessary condition for ensuring the identity of the kinematics of the flow during reversal) (Figure 1).

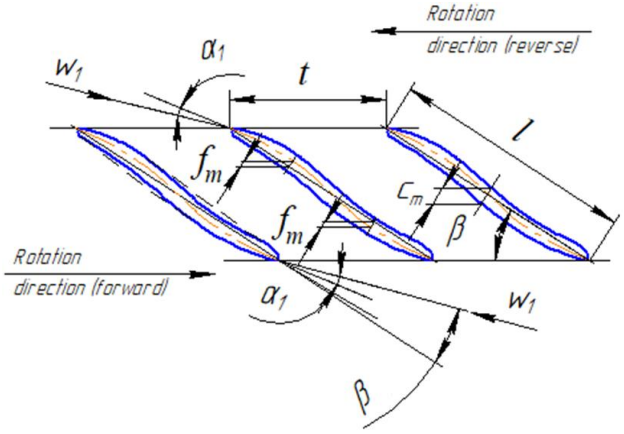

Figure 1 – The reverse pumping grid

For the impeller RK-2, a symmetrical profile [12] has been adopted (Figure 1, dashed line).

The following signatures are used Q – flow rate, m^3/s; H – pressure head, m; n – rotational speed, s^{-1}; r – location radius, m; l – blade length, m; t – blade step, m; β – the angle of the profile installation in the grid, °; α_1 – the angle-of-attack, °; W_1 – relative velocity at the inlet, m/s; f_m – maximum relative curvature of the profile, m; c_m – maximum relative profile thickness, m.

The design parameters of the impellers are presented in Table 1.

The impellers were tested on a hydraulic bench in a cylindrical chamber. The liquid was supplied to and away from the impellers in the axial direction.

The hydraulic characteristics of the tested impellers are presented in Figure 2.

The characteristics were taken at the calculated position of the vane with a rotation angle of $V = 0$. Since the RK-1 did not provide the design parameters for Q and H, it was also tested at $V = 4°$.

The characteristics of the elementary reversible grids are obtained by probing the flow before the impeller and behind them with five-channel ball probes.

Table 1 – The design parameters of the impellers

Impeller	Q, m^3/s	H, m	n, s^{-1}	Section view	r, m	l, m	l/t	β, °	α_1, °	f_m	c_m/l
RK-1	0.17	10	50	Peripheral	0.1150	0.200	1.39	12.8	2.8	0.020	0.040
				Mid	0.0925	0.185	1.59	17.5	5.3	0.030	0.060
				Root	0.0700	0.155	1.76	27.6	11.5	0.040	0.080
RK-2	0.17	10	50	Peripheral	0.1150	0.180	1.00	15.4	4.6	0.015	0.045
				Mid	0.0925	0.160	1.10	19.4	6.0	0.022	0.070
				Root	0.0700	0.140	1.30	26.0	8.6	0.030	0.095

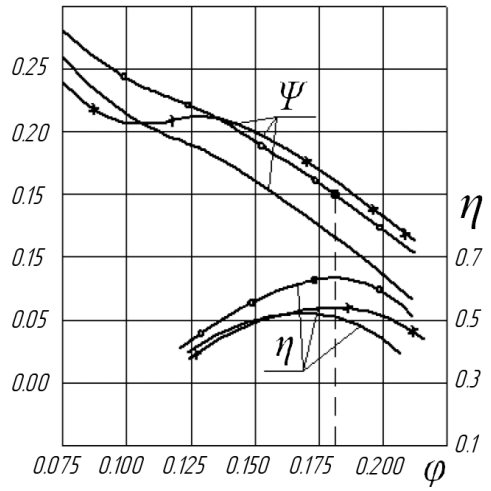

Figure 2 – Hydraulic characteristics of reversible impellers: Ψ – actual head coefficient; η – efficiency; φ – estimated flow (RK-1, $V = 0°$; RK-1, $V = 4°$; RK-2, $V = 0°$)

Probing was carried out in a wide range of flow changes, including such characteristic modes as the calculated mode (mode A), the optimal efficiency mode, and the unstable operation mode (mode B; In the area of pressure-flow characteristic "failure").

Simultaneously, the rotation frequency $n = 50\ s^{-1}$ was kept constant, provided the Reynolds number (flow turbulence) (Reynolds number $Re = (4.6–5.6)\cdot10^4$ was calculated from the total flow rate and diameter of the probe ball). The indicated value of Re was in the range of $(0.04–1.50)\cdot10^5$, i.e., the condition for the constancy of the calibration coefficients of the ball probes was fulfilled [12].

The probes measured the flow in front of the impeller at a distance of $0.65t$ pitch from the blade's leading edge and behind the impeller at a distance of pitch from the trailing edge, where the velocities are almost equalized. The measurements were carried out at eight points along the radius. The extreme measurement points were spaced from the chamber walls and the sleeve by a distance equal to the diameter of the probe ball.

The reliability of the experimental data was verified by comparing the flow rate determined by probe measurements:

$$Q_3 = 2\pi \int_{r_{вт}}^{R} V_z(r) r dr, \quad (1)$$

where V_z – the flow rate component of velocity; R – the outer radius of the impeller, at the inlet and outlet of the impeller with the corresponding flow rates measured by the narrowing device (diaphragm), Q. Typically, the divergence between Q_3 and Q_c was ±3 % before the impeller and ±5 % behind it.

Based on the probing results, the parameters of reverse wheels were determined, particularly the discharge flow coefficient:

$$\varphi = \frac{4Q_2}{\pi D^2(1-\overline{d_{вт}^2})u_R}, \quad (2)$$

the head coefficient:

$$\psi = \frac{2gH}{u_R^2}, \quad (3)$$

and energy efficiency parameters of the elementary grids, i.e., the discharge flow coefficient at input "1" and output "2", respectively:

$$\varphi_{1k} = \frac{V_{1z}(r)}{u_R};\ \varphi_{2k} = \frac{V_{2z}(r)}{u_R}, \quad (4)$$

where $V_{1z}(r)$, $V_{2z}(r)$ – the flow rate component of velocity on the radius of the grid r;

The head coefficient:

$$\psi_k = \frac{2gH_k(r)}{u_R^2}; \quad (5)$$

the grid efficiency:

$$\eta_k = \frac{H_k(r)}{H_p(r)}, \quad (6)$$

where $H_k(r)$ – actual increment of the flow specific energy at radius r, m; $H_p(r)$ – the elementary grid head determined by the flow calculation, m.

Since the non-uniformity of the flow was considered increased, the radius of the jet behind the impeller was r_2 along with the radius of the jet in front of the impeller r_1 from the equal flow rates between the jet and the chamber wall. The parameters of the elementary grid were determined in the cylindrical section at the middle radius between r_1 and r_2. The resulting error was not taken into account, as the radii differed insignificantly and could not make inaccuracies in the calculation exceeding the error of the probe measurements themselves.

In the calculation of the grid parameters, we used the adjusted axial velocities, for which the velocities V_{1z} and V_{2z} were multiplied by the coefficients, respectively:

$$\lambda_1 = \frac{Q_c}{2\pi\int_{r_b}^{R} V_{1z}(r)rdr}; \quad (7)$$

$$\lambda_2 = \frac{Q_c}{2\pi\int_{r_b}^{R} V_{2z}(r)rdr}, \quad (8)$$

where r_b – bushing's radius, m.

The noted parameters of the elementary grids were represented by functions of the relative height of the channel $(r - r_b)/(R - r_b)$ angle of attack α_1.

The parameters of individual elementary grids, presented as a function of the relative height of the channel, made it possible to judge the matching of the blade sections in the radial direction, and the parameters represented as a function of the angle of attack α_1, showed changes in the various parameters with varying flow rates.

In particular, to avoid subjective curves in drawing graphs, Figures 3–5 provided a computer selection of the degree of the averaging polynomial.

3 Results and Discussion

Figure 2 shows the total characteristics of the impellers "$\Psi - \varphi$" and "$\eta - \varphi$". As follows from the figure, for RK-1 with the calculated flow coefficient $\varphi = 0.18$, the experimental value of the Head Coefficient $\Psi = 0.12$ is much less than the calculated $\Psi = 0.15$. The divergence is approximately 20 %. This calls into question the correctness of the lifting forces method for calculating the reverse grids of S-shaped profiles if the grid influence is considered according to the Schilzanzl graphs [1]. Using the method in this form does not provide the required impeller head.

The impeller RK-1 achieves the design head values with lower (compared to the calculated) flow rate factors and higher efficiency. In other words, the liquid receives the necessary energy increment at more significant than the calculated angles of attack α_1, and this process is performed with less hydraulic losses.

When the blades turn from $V = 0°$ to $V = 4°$, the impeller pressure increases (as expected). So, in the mode of calculated flow ($\varphi = 0.18$), the actual head coefficient $\Psi = 0.16$ against calculated $\Psi = 0.15$. The efficiency also increased from $\eta = 0.51$ to $\eta = 0.34$. However, the shape of the head-flow characteristic is deteriorating: its "failure" appears in the partial flow zone. (0.085–0.130).

At the impeller RK-2, a reasonably good agreement was observed between the experimental and calculated head coefficients. At the calculated $\varphi = 0.18$, the numerical values of these coefficients differ by no more than 5 %. Based on this, it can be argued that the numerical optimization method [5] using a computer allows you to design reversed impellers for the specified parameters.

Since the impeller RK-2 was designed with efficiency optimization, the impeller's level in the flow coefficient change range was substantially higher than that of the RK-1. In the calculated mode, it was 0.64.

Observed for RK-1 at $V = 4°$ the "fall-in" of the curve "$\Psi - \varphi$" in the range of $\varphi = 0.085$–0.130 indicates a significant change in the picture of a steady, smooth flow around the blades. In more detail, the research reveals the existence of the separated flows at the blade surface in this zone (Figure 5).

It was possible to establish how hydraulic losses in the flow washing elementary reversiblep grids, angle of attack α_1, level of loading of the blade element (measured by the coefficient Ψ_k), and secondary flows, including overflow in the radial clearance at the periphery of the impeller.

From Figure 3, it follows that for the peripheral and middle sections, there are optimal values of the angles of attack α_1. When changing in one direction or another, the value η_k decreases. Besides, the specified angles do not coincide with the calculated angles (Table 1). A relatively more significant mismatch is observed for RK-1.

Here, these angles are much larger than the calculated ones, which agrees with the total characteristic "$\eta - \varphi$" (Figure 2).

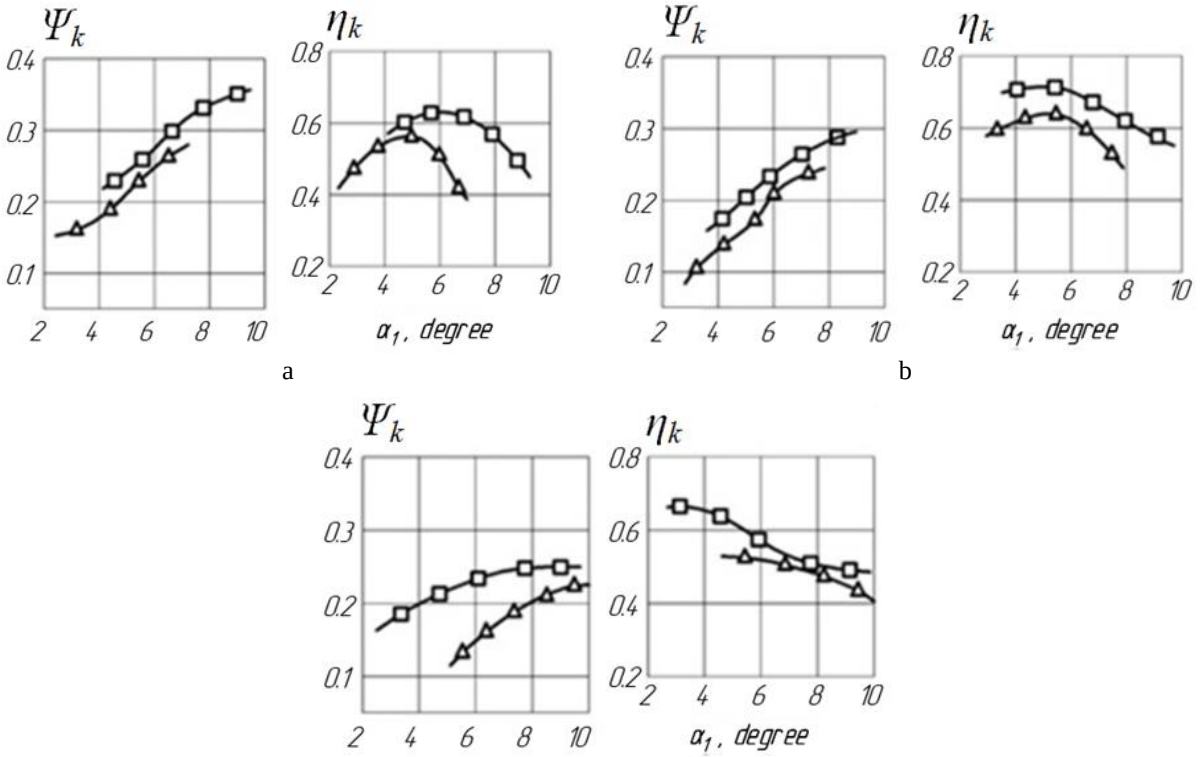

a b c

Figure 3 – The characteristics of the elementary grids in non-cavitation operation conditions: a – the peripheral cross-section; b – the middle section; c – the root section (RK-1, V = 0°; RK-1, V = 0°)

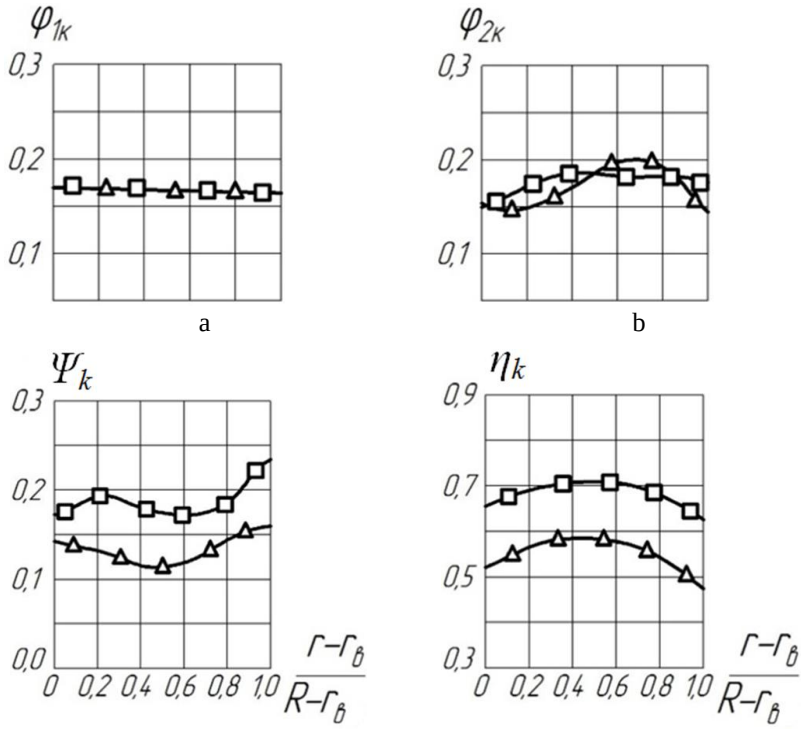

a b c d

Figure 4 – The radius distribution of the parameters of elementary gratings with a calculated flow rate V = 0° (RK-1, φ = 0°, 180°; RK-2, φ = 0°, 180°)

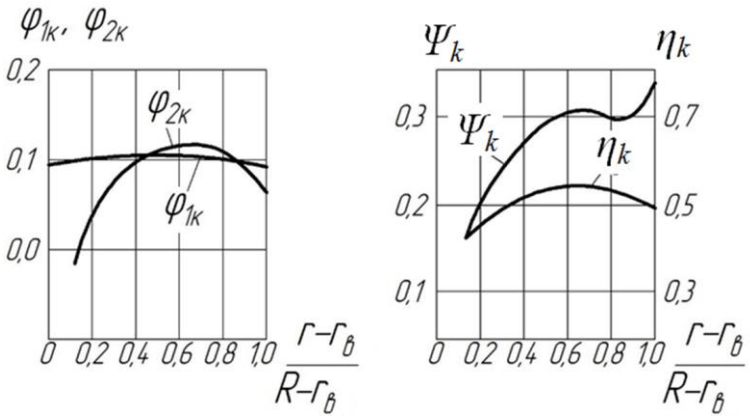

Figure 5 – The radius distribution of the parameters of the elementary grid RK-1 in partial flow rate mode $\varphi = 0.105$ and $V = 4°$

In the direction of the large angles of attack compared with the calculated, the optimal efficiency of the named impeller is shifted.

For RK-2 experimental and design α_1, all sections differ slightly. In the middle section, they are almost the same. This explains a resonably good coincidence of the design and optimal operating modes of the impeller RK-2 (Figure 2).

An analysis of the "$\eta_k - \alpha_1$" curves for RK-2 in the range of the angle-of-attack changes corresponding to the zone of optimal efficiency shows that the η_k on the periphery is by 6–8 %, less than the value of this parameter in the middle blade and by 2.0–2.5 % less than that of the sleeve. Such an increase in energy loss in the end sections of the blade was due to overflows in the radial gap and other secondary flows in this area.

The minimum efficiency η_k noted near the impeller sleeve RK-1 is presumably related to the large thickness of the boundary layer and its possible separation from the blade surface [18].

One of the questions during the research was to determine the permissible load on the blade to take it into account when developing new designs. Based on the obtained experimental data, for the best η_k operation modes of RK-2, it is possible to recommend $\Psi_k = 0.26$–0.29 – for peripheral sections and $\Psi_k = 0.15$–0.17 – for sleeve ones. In this case, the efficiency of the reversing impeller should be expected to be about 0.65–0.66.

Two characteristic modes were selected to represent the radial distribution of parameters across the blade elements: design flow mode (Figure 4) and unstable operation mode (Figure 5). From Figure 5, it can be seen that at the sleeve RK-1, the flow coefficient φ_{2k} is zero or negative. Such a redistribution of the axial velocities indicates the existence of a vortex zone in this region. This is confirmed by visual observations of the flow in stroboscopic lighting (data not shown).

Based on the previous, we have presented a picture of the current around the blade and thus explain the flooding of the head-flow characteristic of the RK-1 impeller at $V = 4°$ in the modes of frequency flows $\varphi = 0.085$–0.130 (Figure 2). Figure 2 shows that with a decrease φ from 0.130 to 0.105 the head Ψ coefficient decreases from 0.212 to 0.205, which may be associated with the formation of the vortices at the sleeve. The presence of such as the flow is further reduced ($\varphi < 0.105$) facilitates the flow conditions of the rest of the blade (since the velocities are redistributed over the height of the channel), which increases from the head.

4 Conclusions

Thus, the economy of the best-tested reverse impeller was 0.63–0.64. The indicated low level of efficiency (compared to the conventional axial wheels is non-reversible) is explained primarily by the strong influence of secondary flows due to the existence of the significant alternating pressure gradients of the head coefficient Ψ_k (Figure 4). An important reason for this was also the possible profile separation of the flow, to which the reversible grids in question are most predisposed.

The presence of alternating gradients of the head coefficients does not recommend any acceptable law of load change along the radius for newly designed reverse pump wheels. This issue needs further study.

To improve the performance of the reversible impellers. It is necessary for a more in-depth study of the effects of secondary flows. Of undoubted interest in this regard are identifying the influence of typical impeller's parameters, length of the blade profile, and the load distribution along the radius on the manifestation of three-dimensional effects.

5 Acknowledgment

The research was carried out at the Research and Educational Center for Industrial Engineering within the R&D project "Fulfillment of tasks of the perspective plan of development of a scientific direction "Technical sciences" Sumy State University" by the Ministry of Education and Science of Ukraine (State reg. no. 0121U112684).

The authors also appreciate the International Association for Technological Development and Innovations for the support during the research.

References

1. Grätzer, G. (1978). *General Lattice Theory*. Basel, Stuttgart: Birkhäuser, doi 10.1007 / 978-3-0348-7633-9.
2. Truijen, D. P. K., De Kooning, J. D. M., Stockman, K. (2021). Drivetrain architectures for a mechanically decoupled contra-rotating reversible pump-turbine. *IEEE/ASME International Conference on Advanced Intelligent Mechatronics*, art. no. 21128193, doi: 10.1109/AIM46487.2021.9517403.
3. Zhu, D., Xiao, R., Liu, W. (2021). Influence of leading-edge cavitation on impeller blade axial force in the pump mode of reversible pump-turbine. *Renewable Energy*, Vol. 163, pp. 939-949, doi:10.1016/j.renene.2020.09.002.
4. Liu, Y., Gong, J., An, K., Wang, L. (2020). Cavitation characteristics and hydrodynamic radial forces of a reversible pump-turbine at pump mode. *Journal of Energy Engineering*, Vol. 146(6), 713, doi: 10.1061/(ASCE)EY.1943-7897.0000713.
5. Johnson, J. L., Leone, F. C. (1977). *Statistics and Experimental Design in Engineering and the Physical Sciences*. John Wiley & Sons, New York.
6. Meng, F., Li, Y., Yuan, S., Wang, W., Zheng, Y., Osman, M. K. (2020). Multiobjective combination optimization of an impeller and diffuser in a reversible axial-flow pump based on a two-layer artificial neural network. *Processes*, Vol. 8(3), 309, doi: 10.3390/pr8030309.
7. Huang, J., Zheng, Y., Kan, K., Xu, Z., Huang, C., Zhou, G., Du, Y. (2022). Hydraulic characteristics of reverse power generation of axial-flow pump. *Journal of Drainage and Irrigation Machinery Engineering*, Vol. 40(3), pp. 230-237, doi: 10.3969/j.issn.1674-8530.20.0207.
8. Zhang, X., Tang, F., Chen, Y., Huang, C., Chen, Y., Wang, L., Shi, L. (2022). Experimental study on the internal pressure pulsation characteristics of a bidirectional axial flow pump operating in forward and reverse directions. *Machines*, Vol. 10(3), 167, doi: 10.3390/machines10030167.
9. Zhou, Y., Zheng, Y., He, Z., Sun, A., Zhang, F., Wang, H. (2019). Pressure fluctuation and fluid-solid coupling in reverse power generation of large axial flow pump. *Journal of Drainage and Irrigation Machinery Engineering*, Vol. 37(6), pp. 480-485, doi: 10.3969/j.issn.1674-8530.18.0034.
10. Ma, P., Wang, J. (2017). An analysis on the flow characteristics of bi-directional axial-flow pump under reverse operation. *Proceedings of the Institution of Mechanical Engineers, Part A: Journal of Power and Energy*, Vol. 231(3), pp. 239-249, doi: 10.1177/0957650917695447.
11. Kang, C., Mao, N., Pan, C., Zhou, Y. (2016). Turbulent flow characteristics in an axial-flow pump at direct and reverse modes. *Journal of Applied Science and Engineering*, Vol. 19(4), pp. 447-458, doi: 10.6180/jase.2016.19.4.08.
12. Husak, O., Panchenko, V. (2022). *Theory of Hydraulic Machines*. Sumy State University, Sumy, Ukraine.